


ARTICLE

<https://doi.org/10.1038/s42005-019-0203-z>

OPEN

The sound of Bell states

M. Arif Hasan ¹, Lazaro Calderin¹, Trevor Lata¹, Pierre Lucas¹, Keith Runge¹ & Pierre A. Deymier¹

Nonseparable states, analogous to “entangled” states, have generated great scientific interest since the very beginning of quantum mechanics. To date, however, the concept of “classical nonseparability” has only been applied to nonseparable states of different degrees-of-freedom in laser beams. Here, we experimentally demonstrate the preparation and tunability of acoustic nonseparable states, i.e. Bell states, supported by coupled elastic waveguides. A Bell state is constructed as a superposition of elastic waves, each a tensor product of a spinor part and an orbital angular momentum (OAM) part, which cannot be factored as a single tensor product. We also find that the amplitude coefficients of the nonseparable superposition of states must be complex. By tuning these complex amplitudes, we are able to experimentally navigate a sizeable portion of the Bell state’s Hilbert space. The current experimental findings open the door to the extension of classical nonseparability to the emerging field of phononics.

¹Department of Materials Science and Engineering, The University of Arizona, Tucson, AZ 85721, USA. Correspondence and requests for materials should be addressed to M.A.H. (email: mdhasan@email.arizona.edu)

The preparation and control of entangled superposition of states (e.g., Bell states) is an essential ingredient for harnessing the second quantum revolution¹. Nonlocality and nonseparability are two distinctive attributes of entangled states. While nonlocality is a unique feature of quantum states, nonseparability is not. The idea of classical “entanglement,” that is, local nonseparable superposition of states, also known as classical nonseparability^{2–4}, has been discussed in great detail in the field of optics, both from the theoretical and the experimental point of view. Spin and orbital degrees of freedom in laser beams can be in a nonseparable state^{5–12}. Nonseparability among different parties such as orbital angular momentum (OAM), polarization, and radial degrees of freedom or propagation direction of a laser beam has also been achieved^{13–15}. The classical entanglement of laser beams has found applications in quantum information science^{16–18}. In contrast, little attention has been paid to the nonseparability of sound waves.

Remarkable new behaviors of sound, analogous to quantum physics, are emerging from the amplitude of acoustic waves, which under the conditions of symmetry breaking may acquire a geometric phase that leads to non-conventional topology¹⁹. Elastic waves in parallelly coupled one-dimensional (1D) waveguides, with either broken time-reversal or parity symmetry, obey Dirac-like equations and possess spin-like (spinor) topology^{20,21}. The amplitude of these pseudospin elastic waves takes the form of a spinor in the two-dimensional Hilbert space of the direction of propagation along the waveguide. In parallel arrays of elastically coupled 1D waveguides, the amplitude also spans an N -dimensional Hilbert subspace, where N is the number of waveguides, and becomes analogous to OAM degrees of freedom^{22,23}. These two degrees of freedom can be used to create nonfactorizable Bell elastic states in the form of linear combinations of tensor products of OAM and spinor (spin-like) amplitudes. Building on these principles, in the current study, we experimentally realize the nonfactorizable superpositions of elastic states, that is, the acoustic Bell states in a coupled elastic waveguides that are not separable, and tune them over a wide region of the tensor product Hilbert space of the directional spinor and OAM subspaces.

Results

Representation and identification of elastic wave states. We consider a system composed of $N = 3$ nearly identical 1D waveguides coupled elastically along their length (Fig. 1). The propagation of longitudinal modes along the waveguides in the long wavelength limit, that is, the continuum limit, is characterized by the equations of motion:

$$\{H \cdot I_{3 \times 3} + \alpha^2 M_{3 \times 3}\} u_{3 \times 1} = 0, \tag{1}$$

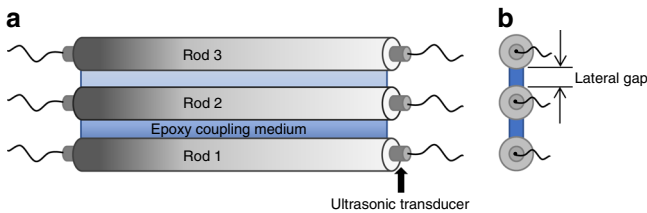


Fig. 1 Experimental coupled elastic waveguides. **a** Side view and **b** front view of the experimental three-rod elastic system designed to support Bell states. The system is composed of three aluminum rods elastically coupled with epoxy (lateral gap of 2 mm). A set of three transducers are used to drive the system at one end. Three more transducers are used as detectors at the other end. Rubber bands are used to maintain a constant pressure on the transducers. Honey is employed as ultrasonic couplant between the transducers and the rods

where the propagation of elastic waves is modeled by the dynamical differential operator $H \left(= \frac{\partial^2}{\partial t^2} - \beta^2 \frac{\partial^2}{\partial x^2} \right)$ in the direction x along the waveguides. The sound speed in the waveguide medium is related to the parameter β . The parameter α measures the elastic coupling strength between the neighboring waveguides (here we take α to be the same for all coupled waveguides). $u_{3 \times 1}$ is a vector whose components, u_i ; $i = 1, 2, 3$, define the i th waveguide displacement. $I_{3 \times 3}$ is the 3×3 identity matrix and the elastic coupling matrix $M_{3 \times 3}$ describes the coupling between waveguides. In our experiment, the coupling matrix takes the form: $M_{3 \times 3} = \begin{pmatrix} 1 & -1 & 0 \\ -1 & 2 & -1 \\ 0 & -1 & 1 \end{pmatrix}$ (see Supplementary Note 2).

The generalized Klein–Gordon equation (1) is Dirac factorizable leading to the two equations:

$$\left\{ U_{3 \times 3} \otimes \sigma_1 \frac{\partial}{\partial t} + \beta U_{3 \times 3} \otimes (-i\sigma_2) \frac{\partial}{\partial x} \pm i\alpha U_{6 \times 6} \sqrt{M_{3 \times 3}} \otimes \sigma_1 \right\} \Psi_{6 \times 1} = 0. \tag{2}$$

In Eq. (2), the antidiagonal matrices are $U_{3 \times 3}$ and $U_{6 \times 6}$ with unit elements. $\sigma_1 = \begin{pmatrix} 0 & 1 \\ 1 & 0 \end{pmatrix}$ and $\sigma_2 = \begin{pmatrix} 0 & i \\ -i & 0 \end{pmatrix}$ are the Pauli matrices, and $\Psi_{6 \times 1}$ is a six-dimensional vector. The modes of vibration of the coupled three waveguides (Fig. 1) are represented by $\Psi_{6 \times 1}$ projected in the two possible (forward and backward) directions of propagation. The $\sqrt{M_{3 \times 3}}$ is not unique. Since the eigen vectors of $\sqrt{M_{3 \times 3}}$ are also the eigen vectors of $M_{3 \times 3}$ itself; this non-uniqueness does not affect in the calculation of the elastic modes of the waveguides of Eq. (2). Let us take the solution of $\Psi_{6 \times 1}$ in the form of plane waves $\psi_I = a_I e^{ikx} e^{i\omega t}$, $I = 1, \dots, 6$, where k is the wave number, ω is the angular frequency, and $a_{6 \times 1}$ is the amplitude vector. The amplitude can be written as $a_{6 \times 1} = e_{n, 3 \times 1} \otimes s_{2 \times 1}$, where $e_{n, 3 \times 1}$ and λ_n are the n th eigen vector and eigen values of $\sqrt{M_{3 \times 3}}$, respectively. Here, the matrix $M_{3 \times 3}$ as well as its corresponding eigen values and vectors are consistent with the concept of OAM of elastic waves traveling along the elastic system of Fig. 1. The three OAM eigen vectors corresponding to the eigen values of $\lambda_1 = 0$, $\lambda_2 = 1$, and $\lambda_3 = 3$ are:

$$e_1 = \frac{1}{\sqrt{3}} \begin{pmatrix} 1 \\ 1 \\ 1 \end{pmatrix}, e_2 = \frac{1}{\sqrt{2}} \begin{pmatrix} 1 \\ 0 \\ -1 \end{pmatrix}, e_3 = \frac{1}{\sqrt{6}} \begin{pmatrix} 1 \\ -2 \\ 1 \end{pmatrix}.$$

The spinor $s_{2 \times 1}$ is solution of the equation:

$$\begin{pmatrix} \omega_n - \beta k & \pm \alpha \lambda_n \\ \pm \alpha \lambda_n & \omega_n + \beta k \end{pmatrix} \begin{pmatrix} s_1 \\ s_2 \end{pmatrix} = 0. \tag{3}$$

From the above eigen equation (3), we find the dispersion relation as $\omega_n^2 = (\beta k)^2 + \lambda_n(\alpha)^2$ and the spinor eigen vectors as $s_{2 \times 1} = s_0 \begin{pmatrix} \sqrt{\omega_n + \beta k} \\ \pm \sqrt{\omega_n - \beta k} \end{pmatrix}$, which is projected into the space of propagation directions. The spinor components are dependent on each other through the wave number k and form a coherent superposition of states in the space of two possible (forward and backward) propagation directions. These spinor components physically correspond to quasi-standing waves, that is, the characteristics of true standing wave at wave number $k = 0$ and the characteristics of true traveling wave as $k \rightarrow \infty$.

As mentioned before, the experimental realization requires a mechanical system, which elastic wave behavior is effectively described by Eq. (1). We, therefore, develop a model of the experimental system by starting with a discrete mass spring

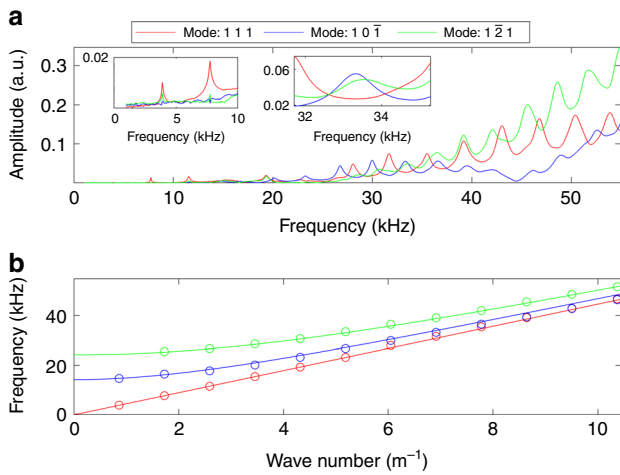


Fig. 2 Identification of elastic wave states. **a** Transmission spectrum of the coupled waveguides for the three orbital angular momentum (OAM) eigen modes e_1 (red), e_2 (blue), and e_3 (green). The inset on the left shows the transmission amplitudes at low frequency < 10 kHz, identifying the first two resonances of the e_1 mode and very low transmission of the other two modes. The inset on the right focuses on a frequency interval showing nearly overlapping e_2 and e_3 resonances and a trough between two resonances in the e_1 transmission around 33.25 kHz. The transmission amplitude is in arbitrary units. **b** Band structure of the coupled waveguides system. The dispersion curves are obtained by fitting the identifiable resonances (open circles) to dispersion relations with cutoff frequencies $\omega_0 = 0, 14.23,$ and 24.27 kHz, respectively

model, which in the long wavelength limit approaches the continuum system (see Supplementary Note 2). The experiment is carried out by first stimulating the coupled waveguides with each of the OAM eigen vectors at one end of the rods and collecting the transmission recorded by transducers at the other end of the rods (see Fig. 1). The experimental setup is devised to explore only longitudinal modes in the system (see Methods and Supplementary Note 3). The finite length rods show resonant peaks in the transmission that are dependent on the mode of stimulation (Fig. 2a). The frequency spectrum of the first OAM eigen mode e_1 of Fig. 2a (mode 1 1 1: red) shows well-defined resonances corresponding to the standing wave modes supported by the finite coupled waveguides. The wavelength corresponding to these standing waves can be easily determined from the expression $\lambda = 2L_e/n$, where n is an integer. Here it is straightforward to assign a value of n to each mode as the observed resonant modes span the complete range of frequencies and their frequency separation is almost uniform. A wave number can subsequently be calculated as $k = 1/\lambda$. Figure 2b shows the resultant dispersion relation by combining data from spectra of Fig. 2a. The speed of sound of the nearly one-dimensional rod is extracted by fitting the low-frequency resonant modes to a linear relation passing through the origin, which is a dispersion relation: $\omega_{k,1} = \beta k$. We find that $\beta = 4467$ m s $^{-1}$.

The second and third OAM eigen modes (e_2 and e_3) (mode 1 0 1: blue and mode 1 2 1: green of Fig. 2a) exhibit transmission spectra that differ from that of the first eigen mode. Both spectra show a significant depression in the transmission amplitude below around a cutoff frequency, namely, 14.23 kHz for e_2 and 24.27 kHz for e_3 . Above the cutoff frequencies, the transmission spectra show well-defined resonances with non-uniform frequency spacing. The resonances are spaced more closely at low frequency.

To calculate the dispersion relation of the second and third bands, $\omega_{k,m}^2 = (\beta k)^2 + \lambda_m(\alpha_m)^2$, $m = 2, 3$, we need to determine

the wave number (k) associated with each resonant frequency (ω_k) observed in the spectra. Similar to the case of the first band, the wave numbers for the other two bands are also multiples of $2L_e$ (due to the finite length of the rods that only support standing waves). Therefore, we label each resonance with the lowest resolvable frequency as being $m = 1$ and rewrite the dispersion relation as $\omega_{k,m}^2 = \beta^2 \Delta k^2 (m_0 + m)^2 + \lambda_m(\alpha_m)^2$, $m = 2, 3$. We then determine the cutoff frequency α_m and the associated m_0 from the frequency resonances ($\omega_{k,m}$) from Fig. 2b. Using Matlab's least-squares fitting procedure, we numerically obtain $(\alpha_2, m_0) = (14.23$ kHz, 0) and $(\alpha_3, m_0) = (24.27$ kHz, 1). The cutoff frequencies are consistent with the measured transmission spectra of Fig. 2a. The dispersion relations are reported in Fig. 2b. The transmission spectra associated with the e_2 and e_3 modes clearly show very low transmission below the cutoff frequency. These resonances correspond essentially to separable states.

Nonseparability of states. Equation (2) is linear, and hence the solution of Eq. (2) can also be obtained by the superposition of modes. It is therefore possible to construct the nonseparable superposition of isofrequency states in the bands corresponding to the two non-zero OAM eigen values:

$$\Psi_{6 \times 1} = A e_2 \otimes \begin{pmatrix} \sqrt{\omega + \beta k_2} \\ \pm \sqrt{\omega - \beta k_2} \end{pmatrix} e^{i k_2 x} e^{i \omega t} + B e_3 \otimes \begin{pmatrix} \sqrt{\omega + \beta k_3} \\ \pm \sqrt{\omega - \beta k_3} \end{pmatrix} e^{i k_3 x} e^{i \omega t}. \quad (4)$$

In Eq. (4), A and B are the Bell state complex coefficients and we have chosen $\omega_2 = \omega_3 = \omega$. k_2 and k_3 are the wave numbers corresponding to the modes in the two bands with same frequency ω . In the superposition of Eq. (4), the eigen vectors of the OAM (e_2, e_3) and the spinor amplitudes are different. This superposition of nonseparable states cannot be written in the form of a tensor product of one spinor and one OAM eigen vector.

For experimental realization of Bell elastic states given by Eq. (4), we consider isofrequency states. To excite such a nonseparable state, we need to identify a frequency at which there is substantial transmission for OAM eigen vectors e_2 and e_3 , but little transmission for e_1 . The right inset of Fig. 2a shows that these conditions are satisfied at a frequency of 33.25 kHz. Therefore, to create a nonseparable superposition of eigen modes e_2 and e_3 , we drive the coupled waveguide system at 33.25 kHz by exciting rods 1 and 2 out of phase, that is, a phase difference of π , and not exciting rod 3. Furthermore, we anticipate that the contribution from these two eigen modes (A and B) can be manipulated by varying the ratio of the amplitude of excitation of rods 1 and 2. The driving amplitudes of rods 1, 2, and 3 are therefore represented by the vector $(F_1, -F_2, 0)$ with the amplitude ratio of the excitation given by $r = |F_1/F_2|$. Figure 3a shows the phase difference between the transmission of each pair of rods as a function of r . We do, indeed, see that manipulation of the excitation amplitude ratio can be used to tune the eigen mode superposition.

We determine the Bell state coefficients, A and B , in Eq. (4), for the three excitation amplitude ratios: $r = 0.0944, 0.4356,$ and 1 corresponding to the states labeled (i), (ii), and (iii) and reported in Fig. 3b. Remarkably, we find that if we fix B to be a real number, we need to allow A to be a complex number to obtain the phases observed in the experiment. In particular, for the three illustrated ratios, we find the following values of $A^{(i)} \approx 0.00496 e^{i \frac{2\pi}{16}}$, $A^{(ii)} \approx 0.00627 e^{i \frac{2\pi}{8}}$, and $A^{(iii)} \approx 0.01640 e^{i \frac{2\pi}{32}}$ with an estimated experimental uncertainty of $\frac{1}{62} \pi$ in $\arg(A)$, and $B^{(i)} \approx 0.00377$, $B^{(ii)} \approx 0.00751$, and $B^{(iii)} \approx 0.01433$ (see

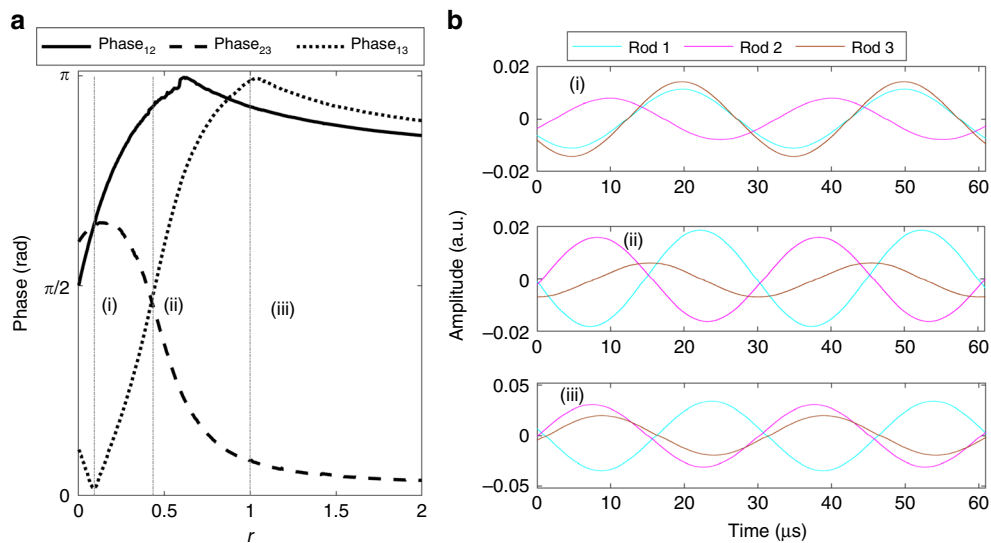


Fig. 3 Measurement and tunability of nonseparable Bell state. **a** Variation of the phase difference between pairs of rods of the coupled waveguides as a function of the ratio of the excitation amplitude of rod 1 to the excitation amplitude of rod 2, r . The third rod is not excited. The vertical lines labeled (i), (ii), and (iii) correspond to ratios $r = 0.0944$, 0.4356 and 1 , respectively. **b** Amplitude versus time recorded by the detecting transducers at the end of each rod corresponding to the three driving amplitude ratios labeled in the left panel. The driving frequency is 33.25 kHz

Methods for details). We calculate the entropy of “entanglement,” $S(\rho_{\text{OAM}})$, for the states labeled (i), (ii), and (iii), and we find $S(\rho_{\text{OAM}})^{(i)} = \frac{15}{16} \ln 2$, $S(\rho_{\text{OAM}})^{(ii)} = \frac{31}{32} \ln 2$, and $S(\rho_{\text{OAM}})^{(iii)} = \frac{63}{64} \ln 2$ (see Supplementary Note 1).

The complex coefficients of the driven Bell state arise naturally from the Lorentzian character of the resonances. This astonishing result indicates that the coefficients for our Bell elastic state can be tuned through the modification of a single input, the relative excitation amplitudes of rods 1 and 2, allowing us to navigate a sizeable portion of the nonseparable states in the tensor product Hilbert space of the directional and OAM subspaces. Further, we expect that the full gamut of possible phases and, hence, the full range of complex A could be explored through more elaborate excitation schemes.

Discussion

Using a classical system in the current work, we have been able to capture the characteristic of nonseparability between different degrees of freedom of the same physical manifestation. The experimental realization of these nonseparable superpositions of elastic states, that is, the Bell states consisted of a set of coupled elastic waveguides. We further quantified the Bell state and to our surprise we found the coefficients must be complex. By tuning these complex coefficients, we were able to experimentally navigate a sizeable portion of the nonseparable states. The stronger coupling, available in the considered acoustic system with the use of epoxy coupling medium, allowed us to realize the full benefit of a much wider scope of possible relationships in the acoustic coherent superpositions.

The experimental demonstration of the acoustic Bell state in a parallel array of three elastically coupled waveguides opens the door to the extension of the notion of classical nonseparability to the emerging field of phononics. The ability to prepare and tune the complex amplitudes of the nonseparable superposition of elastic states by exciting the waveguides with the appropriate combination of frequency, phase and amplitude suggests that elastic waves may offer a classical alternative to true quantum systems in some quantum information processing applications.

Methods

Sample fabrication. The experimental sample (coupled acoustic waveguide) is composed of three (nearly) identical aluminum rods of $d = 1/2$ in. diameter and length $L = 0.6096$ m with a density of 2660 kg m^{-3} (6061 aluminum with certification: McMaster-Carr 1615T172). The rods are coupled elastically by filling the 2 mm gap that separates them with epoxy (J.-B. Weld 50176 KwikWeld Steel Reinforced Epoxy) along the length of the rod (cf., Fig. 1). Special care was taken to ensure a uniform gap between the rods and a uniform filling along the rods. The length of the epoxy filling is $L_e = 0.5786$ m.

Experimental details. We have used different types of attachments of the transducers (Olympus V133-RM Fingertip case style with $1/4$ in. element diameter) to the ends of the rods as well as different ultrasonic couplants. However, the observed elastic modes are essentially invariant, and the couplant and attachment method only affect the number of modes that can be resolved. Optimal resolution of the elastic modes is achieved by wrapping rubber bands (supersize bands from Walmart, 564755837) around the transducer/rod assembly and employing honey as ultrasonic couplant between the transducers and the rods. The layer (thickness) of couplant on the surface of the sample was kept constant by maintaining a uniform pressure on the transducers throughout all experiments. Moreover, the use of rubber bands better eliminated trapped air from the contact region of the transducer/rod assembly. Since honey provides high acoustic impedance (due to its high viscosity that contributed to its acoustic impedance of 2.89 MPa m^{-2} , whereas the acoustic impedance of the experimental aluminum rods is 11.88 MPa m^{-2}), it produces better transmission of sound waves into the waveguides. Furthermore, the use of honey couplant in conjunction with the longitudinal wave transducers suppress all non-longitudinal modes (torsional, transversal, etc.) of the aluminum waveguides, as shown in Supplementary Fig. 1 in the Supplementary Note 3 for $N = 1$ free standing aluminum rod.

Preparation of a Bell state. The resonances shown in Fig. 2 correspond essentially to separable states. To realize Bell elastic states we need to form an isofrequency nonfactorizable linear combination of tensor products of the OAM and spinor degrees of freedom. To create such a nonseparable state, we have identified a frequency, 33.25 kHz, at which there is substantial transmission for the OAM eigen vectors e_2 and e_3 , but little transmission for e_1 . Driving the system at that frequency will result in near-resonant excitations of the e_2 and e_3 modes and very weak resonant amplitudes for the e_1 mode.

Bell state measurement and tenability. The spinors in Eq. (4) correspond to quasi-standing elastic waves with the components of the spinor representing the amplitude of the wave in the forward and backward directions of propagation, respectively¹⁸. However, due to the finite length of the experimental waveguides, the spinor components need to be converted to standing waves. The Bell state given by Eq. (4) can be generalized by superposing solutions for positive and negative

wave numbers:

$$\Psi_{6 \times 1} = Ae_2 \otimes \begin{pmatrix} \sqrt{\omega + \beta k_2} e^{ik_2 x} + \sqrt{\omega - \beta k_2} e^{-ik_2 x} \\ \pm \sqrt{\omega - \beta k_2} e^{ik_2 x} \pm \sqrt{\omega + \beta k_2} e^{-ik_2 x} \end{pmatrix} e^{i\omega t} \\ + Be_3 \otimes \begin{pmatrix} \sqrt{\omega + \beta k_3} e^{ik_3 x} + \sqrt{\omega - \beta k_3} e^{-ik_3 x} \\ \pm \sqrt{\omega - \beta k_3} e^{ik_3 x} \pm \sqrt{\omega + \beta k_3} e^{-ik_3 x} \end{pmatrix} e^{i\omega t}. \quad (5)$$

The spinor components represent standing wave displacements in the finite rods if the wave numbers k_2 and k_3 are integer multiples of $\frac{\pi}{L}$. For the case of isofrequency state at $\omega = 33.25$ kHz, from Fig. 2b we have $k_2 = \frac{2\pi}{L} 8$ and $k_3 = \frac{2\pi}{L} 6$. At that frequency, Eq. (5) when applied to the ends of the rods, $x = L$, where measurements are performed, reduces to the scalar expression:

$$\frac{A}{\sqrt{2}} \begin{pmatrix} 1 \\ 0 \\ -1 \end{pmatrix} \frac{1}{\sqrt{2\omega}} (\sqrt{\omega + \beta k_2} + \sqrt{\omega - \beta k_2}) + \frac{B}{\sqrt{6}} \begin{pmatrix} 1 \\ -2 \\ 1 \end{pmatrix} \frac{1}{\sqrt{2\omega}} (\sqrt{\omega - \beta k_3} + \sqrt{\omega + \beta k_3}) = \begin{pmatrix} C_1 e^{i\phi_1} \\ C_2 e^{i\phi_2} \\ C_3 e^{i\phi_3} \end{pmatrix}. \quad (6)$$

In Eq. (6) we have normalized the spinors. A and B are the Bell state complex coefficients, C_i is the maximum displacement amplitude recorded by the detecting transducer at the end of rod i , $i = 1, 2, 3$, and ϕ_i is the corresponding phases. The right-hand side term of Eq. (6) can be reformulated in terms of the phase difference between the transmission of each pair of rods and for the sake of simplicity (and without loss of generality) assume $\phi_2 = 0$,

$$\begin{pmatrix} C_1 e^{i\phi_{12}} \\ C_2 \\ C_3 e^{-i\phi_{23}} \end{pmatrix},$$

where $\phi_{12} = \phi_1 - \phi_2$ and $\phi_{23} = \phi_2 - \phi_3$. Using Eq. (6), we are able to extract the Bell state, that is, the complex coefficients A and B with an experimental uncertainty of no more than $\frac{1}{64}\pi$.

The coefficients A and B are also functions of the amplitudes (C_i) and phases (ϕ_i) recorded by the detecting transducers at the end of each rod, which are also a functions of the excitation amplitude of the rods as shown in Fig. 3a. Therefore, Eq. (6) also demonstrates how we can tune the eigen mode superposition, that is, the Bell state.

Data availability

The data that support our findings of the present study are available from the corresponding author upon request.

Received: 29 March 2019 Accepted: 31 July 2019

Published online: 05 September 2019

References

- Dowling, J. P. & Milburn, G. J. Quantum technology: the second quantum revolution. *Philos. Trans. R. Soc. Lond. Ser. A* **361**, 1655–1674 (2003).
- Spreeuw, R. J. C. A classical analogy of entanglement. *Found. Phys.* **28**, 361–374 (1998).
- Ghose, P., . & Mukherjee, A. Entanglement in classical optics. *Rev. Theor. Sci.* **2**, 274–288 (2014).
- Karimi, E. & Boyd, R. W. Classical entanglement? *Science* **350**, 1172–1173 (2015).
- Souza, C. E. R., Huguenin, J. A. O., Milman, P. & Khoury, A. Z. Topological phase for spin-orbit transformations on a laser beam. *Phys. Rev. Lett.* **99**, 160401 (2007).
- Chen, L. & She, W. Single-photon spin-orbit entanglement violating a Bell-like inequality. *J. Opt. Soc. Am. B* **27**, A7–A10 (2010).
- Borges, C. V. S., Hor-Meyll, M., Huguenin, J. A. O. & Khoury, A. Z. Bell-like inequality for the spin-orbit separability of a laser beam. *Phys. Rev. A* **82**, 033833 (2010).
- Karimi, E. et al. Spin-orbit hybrid entanglement of photons and quantum contextuality. *Phys. Rev. A* **82**, 022115 (2010).
- Vallés, A. et al. Generation of tunable entanglement and violation of a Bell-like inequality between different degrees of freedom of a single photon. *Phys. Rev. A* **90**, 052326 (2014).
- Pereira, L. J., Khoury, A. Z. & Dechoum, K. Quantum and classical separability of spin-orbit laser modes. *Phys. Rev. A* **90**, 053842 (2014).

- Qian, X.-F., Little, B., Howell, J. C. & Eberly, J. H. Shifting the quantum-classical boundary: theory and experiment for statistically classical optical fields. *Optica* **2**, 611–615 (2015).
- Balthazar, W. F. et al. Tripartite nonseparability in classical optics. *Opt. Lett.* **41**, 5797–5800 (2016).
- Hashemi Rafsanjani, S. M., Mirhosseini, M., Magaña-Loaiza, O. S. & Boyd, R. W. State transfer based on classical nonseparability. *Phys. Rev. A* **92**, 023827 (2015).
- Michler, M., Weinfurter, H. & Żukowski, M. Experiments towards falsification of noncontextual hidden variable theories. *Phys. Rev. Lett.* **84**, 5457–5461 (2000).
- Gadway, B. R., Galvez, E. J. & Zela, F. D. Bell-inequality violations with single photons entangled in momentum and polarization. *J. Phys. B* **42**, 015503 (2008).
- Schmid, C. et al. Experimental implementation of a four-player quantum game. *N. J. Phys.* **12**, 063031 (2010).
- Simon, B. N. et al. Nonquantum entanglement resolves a basic issue in polarization optics. *Phys. Rev. Lett.* **104**, 023901 (2010).
- Pinheiro, A. R. C. et al. Vector vortex implementation of a quantum game. *J. Opt. Soc. Am. B* **30**, 3210–3214 (2013).
- Deymier, P. & Runge, K. *Sound Topology, Duality, Coherence and Wave-Mixing: An Introduction to the Emerging New Science of Sound* (Springer International Publishing, 2017).
- Deymier, P. A., Runge, K., Swintek, N. & Muralidharan, K. Torsional topology and fermion-like behavior of elastic waves in phononic structures. *C. R. Mécanique* **343**, 700–711 (2015).
- Deymier, P. & Runge, K. One-dimensional mass-spring chains supporting elastic waves with non-conventional topology. *Crystals* **6**, 44 (2016).
- Deymier, P. A., Runge, K., Vasseur, J. O., Hladky, A.-C. & Lucas, P. Elastic waves with correlated directional and orbital angular momentum degrees of freedom. *J. Phys. B* **51**, 135301 (2018).
- Deymier, P. A., Vasseur, J. O., Runge, K. & Lucas, P. in *Phonons in Low Dimensional Structures* (2018). <https://doi.org/10.5772/intechopen.77237>.

Acknowledgements

We acknowledge financial support from the W.M. Keck Foundation.

Author contributions

P.A.D. and K.R. conceived the idea of the research and performed the theoretical studies. M.A.H., L.C., and T.L. fabricated the samples, built the experimental setups, and performed the measurements. M.A.H., L.C., P.L., K.R., and P.A.D. analyzed the data. All authors contributed to the scientific discussion and to writing the manuscript.

Additional information

Supplementary information accompanies this paper at <https://doi.org/10.1038/s42005-019-0203-z>.

Competing interests: The authors declare no competing interests.

Reprints and permission information is available online at <http://npg.nature.com/reprintsandpermissions/>

Publisher's note: Springer Nature remains neutral with regard to jurisdictional claims in published maps and institutional affiliations.



Open Access This article is licensed under a Creative Commons Attribution 4.0 International License, which permits use, sharing, adaptation, distribution and reproduction in any medium or format, as long as you give appropriate credit to the original author(s) and the source, provide a link to the Creative Commons license, and indicate if changes were made. The images or other third party material in this article are included in the article's Creative Commons license, unless indicated otherwise in a credit line to the material. If material is not included in the article's Creative Commons license and your intended use is not permitted by statutory regulation or exceeds the permitted use, you will need to obtain permission directly from the copyright holder. To view a copy of this license, visit <http://creativecommons.org/licenses/by/4.0/>.

© The Author(s) 2019